Designing and Deploying a Mobile UVC Disinfection Robot

Alyssa Pierson[1,2], John W. Romanishin[1], Hunter Hansen[1], Leonardo Zamora Yañez[1], and Daniela Rus[1]

***Abstract*— This paper presents a mobile UVC disinfection robot designed to mitigate the threat of airborne and surface pathogens. Our system comprises a mobile robot base, a custom UVC lamp assembly, and algorithms for autonomous navigation and path planning. We present a model of UVC disinfection and dosage of UVC light delivered by the mobile robot. We also discuss challenges and prototyping decisions for rapid deployment of the robot during the COVID-19 pandemic. Experimental results summarize a long-term deployment at The Greater Boston Food Bank, where the robot delivers (nightly) UVC dosages of at least 10 mJ/cm^2 to a 4000 ft^2 area in under 30 minutes. These dosages are capable of neutralizing 99% of coronaviruses, including SARS-CoV-2, on surfaces and in airborne particles. Further simulations present how this mobile UVC disinfection robot may be extended to classic problems in robotic path planning and adaptive multi-robot coverage control.**

I. Introduction

Ultraviolet Germicidal Irradiation (UVGI), a proven technology in hospital disinfection, shows promise in fast and effective neutralization of viruses, bacteria, and many other pathogens and microbes. Ultraviolet-C (UVC) light in the $100 - 280$nm range inactivates microbes by damaging its RNA or DNA, which prevents replication and causes the microbe to die [1]. Since the effectiveness of UVC directly depends on the distance and line-of-sight to a target area, coverage with stationary fixtures may require many units and be prohibitively expensive for large buildings, such as offices and warehouses. In this paper, we present algorithms for mobile UVC disinfection robots, and a platform designed to autonomously map, navigate, and patrol environments while delivering UVC dosages to targeted surface areas and air volumes. Experiments from a deployment at The Greater Boston Food Bank (GBFB) are also discussed.

Solutions for UVGI allow for hands-free and chemical-free disinfection of high-traffic essential service locations, such as hospitals, grocery stores, and food banks. UVC disinfection reduces the risk of transmission by neutralizing surface and airborne pathogens. Unlike chemical-based disinfection, which may not be appropriate for food or sensitive equipment, UVC exposure has no adverse effects on the quality of food [2], can disinfect electronic equipment [3] without damage, as well as other surfaces not suitable for chemical disinfection [4]. However, UVC operates in a line-of-sight mode and exposure can cause skin and eye damage in humans, further necessitating robotic devices.

[1]Computer Science & Artificial Intelligence Laboratory, Massachusetts Institute of Technology, Cambridge, MA 02139, USA [johnrom, hansena, lzamora]@mit.edu , rus@csail.mit.edu

[2]Department of Mechanical Engineering, Boston University, Boston, MA 02215, USA pierson@bu.edu

This work supported in part by the Office of Naval Research (ONR), and NVIDIA. Their support is gratefully acknowledged.

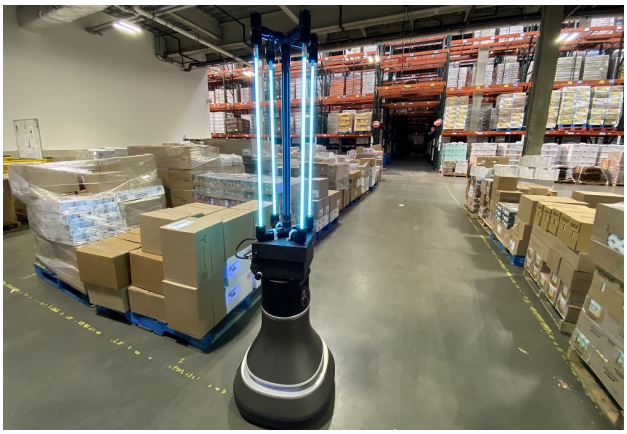

Fig. 1: Our UVC mobile disinfecting robot at The Greater Boston Food Bank. The robot performs nightly autonomous patrols of the aisles of pallets.

The COVID-19 pandemic created an immediate need for this technology at The Greater Boston Food Bank. Food insecurity rose as a result of the pandemic [5], making food banks an essential service that could not afford to shut down. At The GBFB, up to fifty different delivery groups may pass through the warehouse each day, creating a risk of community transmission. UVC disinfection complements the other protocols within The GBFB, such as chemical disinfection, mask-wearing, social distancing, and other best practices. This paper summarizes our system deployment and experiments during 2020. Our system provided additional disinfection to the staging area of the warehouse, approximately 4000 square feet, in under 30 minutes, and ran its autonomous patrols at night when no humans are present.

Shown in Figure 1, our design comprises three components: a mobile robot base, a radial UVC lamp assembly, and algorithms for autonomous operation. The radial design of the UVC lamps provide 360° coverage to disinfect both surfaces and aerosols within the environment. The main contributions of this paper are:

- A model for mobile UVC disinfection of surfaces and aerosols, with algorithms for autonomous patrol;
- Algorithms for patrolling known and unknown environments with one or more robots;
- A mobile UVC disinfection robot platform; and
- Experimental results from The GBFB deployment.

While our initial motivating objective was to mitigate the risk of COVID-19 exposure, our autonomous solution extends to other uses of UVC disinfection. Current applications include food pasteurization and processing [6], [7], medical environment disinfection [8], [9], and laboratory containment systems [10], to name a few. UVC can mitigate exposure to other infectious diseases in public spaces, such as influenza

[11], tuberculosis [12] and pneumonia [13], making it an applicable technology beyond the COVID-19 pandemic.

Related Work

The autonomous UVC disinfection problem is related to a number of classic problems in robotics. We draw inspiration from path-planning algorithms, such as Cellular Decomposition [14], [15] and Task Allocation [16], [17], [18]. Persistent Monitoring strategies [19], [20], [21], [22] can help in designing systems that meet UVC dosage requirements. We also extend to multiple robots with principles from Coverage Control [23], [24], [25], [26].

Several market solutions exist for providing UVC disinfection, which we categorize as: stationary fixtures; mobile carts; and autonomous robotic solutions. Mobile carts differ from robot solutions in that they do not have autonomous navigation capabilities, such as the Xenex [27] mobile device or Surfacide [28] multi-cart solutions. Autonomous robotic solutions offer several key advantages: first, the robots are capable of autonomous navigation between areas of interest. Advanced sensor capabilities enable more precise localization and UVC dosage delivery. These sensors also enable safety features, like automatic shut-off with people detection. One of the first robotic disinfection robots was UVD Robots [29], which is summoned to disinfection zones by a human operator that also initializes disinfection runs. The SmartGuardUV [30] robot uses PURO lamps for pulsed light disinfection, which requires a "stop-and-go" motion. In contrast, our system presented in this paper is designed to autonomously patrol environments without the need for human supervision, with continuous UVC disinfection.

The remainder of this paper is organized as follows: In Section II, we present our model of UVC disinfection for a mobile autonomous robot in environments with occlusions. Section III discusses algorithms for path-planning for one or more robots, with simulations in Section IV. We detail our mobile UVC platform in Section V, discuss our experimental results from The GBFB in Section VI, and present our conclusions in Section VII.

II. Modeling UVC Dosage Delivery

Our models of UVC dosage for a mobile robot are critical to the design of the UVC robot. First, we present a primer on UVC Disinfection and our method for determining the appropriate dosages for microbe and pathogen inactivation. Next, we formulate the mathematical model for how a mobile robot delivers UVC dosages to the environment, including in environments with occlusions, which informs the design of our autonomous algorithms.

A. Basics of UVC Disinfection

Disinfection is commonly modeled with a log-linear model that relates the inactivation rate to the microbial concentration [31]. We relate the disinfection dosages to the required **log reductions**. A 1-log reduction means that 90% of the colony has been inactivated, a 2-log reduction inactivates 99%, a 3-log reduction inactivates 99.9%, and so forth. We refer to the dosages that achieve these log reductions as a D_{90} dose for a 1-log reduction, and a D_{99} dose for the 2-log reduction. UVC disinfection is log-linear with respect to time [6], such that a D_{99} is twice a D_{90} dosage, and takes twice the exposure time from a UVC light source.

B. UVC Dosages for COVID-19 Disinfection

Our primary goal for The GBFB deployment was to mitigate the risk of exposure to COVID-19. To determine our target D_{90} and D_{99} dosage values, we studied both emerging research on UVC susceptibility of SARS-CoV-2, as well as existing research on similar coronaviruses, such as SARS-CoV-1, MHV, and MERS.

At the point of deployment in June 2020, we chose to follow the conservative approximation of 10 mJ/cm^2 for our D_{90} dosage value for surfaces, based on research on similar coronaviruses [32]. Furthermore, we note that airborne particles are more susceptible to UVC irradiation, where a dose of $D_{90} \approx 1$ mJ/cm^2 was reported [33]. More recent studies on SARS-CoV-2 show an even greater susceptibility to UVC irradiation, suggesting a D_{99} dosage of around 5 mJ/cm^2 for SARS-CoV-2 on wet and dried surfaces [34], [35], [36]. Thus, our target dosage is sufficient to provide surface and airborne disinfection about the D_{99} threshold.

C. Modeling the UVC Dosage Footprint

To achieve our target dosage, we need a model of how the robot delivers UVC. For an environment Q, with points denoted $q \in Q$, and the position of our robot p_i, the intensity of UVC light $I(\cdot)$ a point receives is proportional to the inverse squared distance,

$$I(p_i, q) = \frac{\alpha}{\|p_i - q\|^2}, \tag{1}$$

where α is a constant of the UVC lamps. For example, a lamp that $150\mu W/cm^2$ at one meter has an $\alpha = 1.5e6\mu W$. The UVC dosage delivered by the robot is calculated as the intensity over a time interval Δt,

$$D^\tau(p_i, q, \Delta t) = \frac{\alpha}{\|p_i - q\|^2}\Delta t, \tag{2}$$

for $\tau = k\Delta t$ point in time. We account for robot motion and approximate the total dosage over time $D(p_i(t), q, t)$ at a point q by discretizing the trajectory of the robot,

$$D(p_i(t), q, t) = \sum_{\tau=1}^{n} D^\tau(p(t), q, t). \tag{3}$$

We apply (3) to all points in the environment to find the dosage over an area, which we denote $D(p_i(t), Q, t)$ for an area Q. In Section V-B, we detail the specific modeling parameters of our four-lamp assembly, validated by measurements with a UVC dosimeter.

D. Accounting for Occlusions

The effectiveness of UVC disinfection relies on the surface or airborne particle being in line-of-sight to the UVC lamps. Note that (2) and (3) provide the unoccluded dosage: in practice, it is necessary to check that q is not occluded. In Section III, we discuss two approaches that account for occlusions: first, with a lidar sensor, and second by a convex decomposition of the space. Since a lidar sensor returns points within line-of-sight of the robot, we can construct

a visibility footprint and only update our dosage estimates from (2) to points within the footprint.

If the robot is not equipped with a 360° lidar sensor, we can also estimate line-of-sight points by constructing convex regions. For some convex region Ω_j, we know that all points are visible to the robot if the robot is also in the convex region. Calculation of dosage accumulation in (3) is restricted to the convex region containing the robot at that point in time, $D^\tau(p_i, \Omega_j, \Delta t)$. Over an environment with obstacles, we can either decompose the region into m convex regions, where no two regions should overlap, $\Omega_j \cap \Omega_k = \emptyset$. Alternatively, as detailed in Section III, a robot's Voronoi cell V_i is a convex region containing the robot, and so the robot can update its dosage estimates by $D^\tau(p_i, V_i, \Delta t)$.

III. Path Planning and Multi-Robot Coverage

In this section, we present two algorithms for mobile UVC disinfection. First, we present a path-planning algorithm for delivering dosage through a known, static non-convex environment, such as an office environment. Next, we present an adaptive coverage algorithm suitable for environments where the obstacles may change locations between disinfection patrols. The adaptive coverage algorithm draws inspiration from Voronoi-based coverage control, and is extensible to multiple distributed mobile robots. Simulation results of the adaptive Voronoi-based coverage algorithm are presented in Section IV, and the static path algorithm was the basis for experiments performed at The GBFB in Section VI.

A. Optimized Path in Static Environment

Consider an office environment Q, where a robot may be instructed to disinfect offices, but needs to locally navigate around clutter and other obstacles. A human expert may be able to look at the floor plan and identify regions to disinfect, but may not be able to construct an optimal trajectory through the complex space. In this scenario, we assume that the robot has been given a map of the environment, with a task specification of its patrol from the user, such as "visit all eight offices," which the user has annotated on the map. To ensure the desired UVC dosage is delivered to all specified regions, we create a graph representation of the environment $\mathcal{G}_Q = (\mathcal{N}, \mathcal{E})$, where the nodes $\mathcal{N}$ represent locations the robot can visit, and the edges $\mathcal{E}$ denote the path between nodes. Each node contains a dosage requirement, and we fix the speed of the robot and the node spacing, such that if the robot visits a node, it will deliver the required dosage.

To generate the optimized path for the robot, we ran two levels of an $A^\star$ algorithm: first, we search all traversable neighboring nodes to find the shortest path between the entrances to the office regions. Next, a second layer checked all traversable nodes marked to receive UVC disinfection and used a heuristic to consider adjacent nodes first in order to construct a path until all nodes needing UVC disinfection were a part of the robot's planned path.

As the robot traverses its planned path, we calculate the total accumulated dosage. We account for occlusions, walls, and obstacles by leveraging the lidar information to determine what points are within line-of-sight of the robot, illustrated in Figure 2.

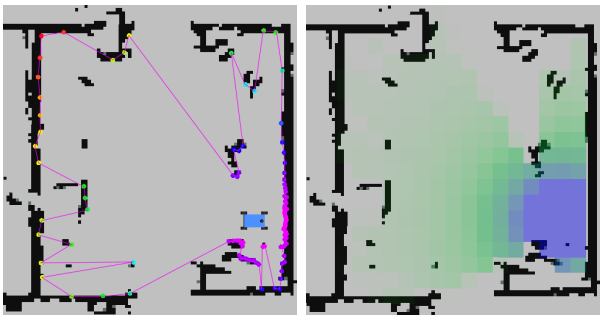

(a) Lidar Footprint (b) Dosage Applied

Fig. 2: (a) Simulation of visible points from the lidar, with the enclosed footprint traced in pink. (b) Dosage applied by the robot, masked by the lidar footprint. Note that the lidar allows us to account for shadows.

By constructing a lidar mask, we create a "visibility footprint" for the dosage calculation. Let Γ_i define the set of points q visible by the lidar of the robot p_i at a given timestep. We define $L_i(p_i(t), q, t)$ as an indicator function,

$$L_i(p_i(t), q, t) = \begin{cases} 1 & \text{if } q \in \Gamma_i(p_i(t), q, t), \\ 0 & \text{otherwise.} \end{cases} \tag{4}$$

In Algorithm 1, this indicator function (4) masks the unoccluded dosage (2). We refer to the entire environment as $L_i(p_i(t), Q, t)$ and $D^\tau(p_i(t), Q, t)$. Let $D^V(p_i(t), Q, t)$ define the dosage applied to all visible points,

$$D^V(p_i(t), Q, t) = \sum_{\tau=1}^{n} L_i(p_i(t), Q, \Delta t) D^\tau(p_i(t), Q, \Delta t). \tag{5}$$

Determining occlusions from lidar sensors is suitable for environments where the obstacles may change over time, or during online re-planning. We summarize the dosage accumulation calculation and the overall static path plan in Algorithm 1.

Algorithm 1 Dosage Calculation from Lidar

1: Identify regions to receive dosage
2: Create Graph of environment $\mathcal{G}_Q$
3: Identify a path connecting all regions
4: Connect all points requiring dosage to generate patrol
5: **while** Robot is on patrol **do**
6: Calculate unoccluded dosage $D^\tau(p_i, Q, t)$ (2)
7: Calculate lidar footprint $L_i(p_i, t)$ (4)
8: Mask dosage with footprint $L_i * D^\tau$
9: Update accumulated dosage D^V (5)

Simulations of Algorithm 1 were performed on an office map, illustrated in Figure 3. In Figure 3a, we illustrate the graph discretization of the environment, used to construct the patrol path. Here, the shaded pink cells correspond to traversable cells within regions the user has specified to visit. Figure 3b illustrates the generated path and total applied dosage to patrol the office regions. The color scale indicates the total dosage: blue regions correspond to UVC dosages

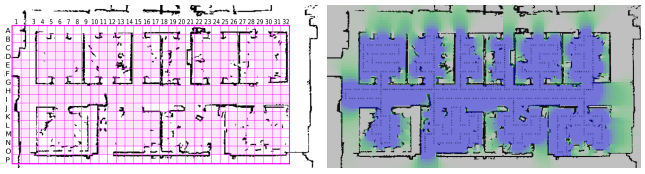

(a) Discretized Environment (b) Dosage Applied Along Path

Fig. 3: (a) Discretized representation of the environment. Pink cells indicate traversable locations marked to receive UVC dosage. (b) From the discretized environment in (a), the robot optimizes its path to deliver dosage to all nodes. The overlay shows the total dosage delivered by the robot.

meeting or exceeding the desired dosage, while the green regions indicate some dosage applied, and gray indicates no dosage applied. As shown, occlusions and obstacles within the offices create shadows and areas that may not receive the total desired dosage. In the next section, we discuss one possible adaptive coverage policy that may address local replanning around obstacles.

B. Adaptive Voronoi-Based Coverage

As the robot performs its UVC disinfection patrols, it may encounter static obstacles that are not included in its map of the environment. Here, we present an algorithm that draws inspiration from Voronoi-based coverage control to navigate an environment with obstacles and adapt online to move towards regions needing UVC dosage. We choose a Voronoi-based approach, as a robot's Voronoi cell provides a local convex sub-region. This sub-region is important for several reasons: first, as a convex cell, we know all points are within line-of-sight, and can readily update our dosage estimation. If the agent plans actions within its Voronoi cell, we know it will also avoid collisions. Finally, this approach scales to a team of distributed robots. We use the Obstacle-Aware Voronoi Tessellation [37] to account for obstacles and maximize the individual cell area.

Traditional Voronoi-based coverage control [23], [24], [25] deploys a team of agents across some environment to minimize a locational cost function. Consider a team of n robots in an environment Q. Points in Q are denoted $q \in Q$, and the positions of the robots are denoted p_i. We define an information density function $\phi(q)$ that specifies the importance of any point. Robots assess the quality of their locations with a locational cost function,

$$\mathcal{H} = \sum_{i=1}^{n} \int_{V_i} \|q - p_i\|^2 \phi(q) dq, \tag{6}$$

where V_i is the Voronoi cell for robot at p_i, and $q \in Q$ is a location in the environment. It can be shown [23] that if each agent moves to the centroid of V_i, $\mathcal{H}$ converges to a local minimum, and all agents reach a static configuration.

We propose that UVC disinfection is analogous to the coverage problem, where $\phi_D(q)$ represents the desired UVC dosage at any point. Instead of the robots optimizing their sensor locations, their task is to optimize their delivery of UVC to points in the environment requiring a UVC dosage. As the robot moves through the environment, we update the required dosage by subtracting the dosage delivered by a robot within its Voronoi cell at each time step,

$$\phi_D(q, t + \Delta t) = \phi_D(q, t) - \sum_{i=1}^{n} D^\tau(p_i, V_i, \Delta t). \tag{7}$$

Note in (7) we restrict D^τ to the robot's Voronoi cell V_i, which underestimates the actual dosage delivered. If the dosage delivered by $D^\tau(\cdot)$ is greater than the dosage required from $\phi_D(q, t)$, then we set the value of $\phi_D(q, t)$ to zero. The function $\phi_D(q, t)$ acts as a "density" function that informs the robots of how much dosage is needed at any point. Continuing this analogy, the "mass" of the environment scores the total missing dosage. We define the mass M_Q:

$$M_Q(t) = \int_Q \phi_D(q, t) dt. \tag{8}$$

Intuitively, by decreasing the mass of the environment, the robot will drive towards regions that need UVC dosage. We assume that our robot(s) have knowledge of $\phi_D(q, t)$ and $M_Q(t)$, which can be estimated by their individual movements and shared position data with other robots in the environment. To decrease $M_Q(t)$, we first identify peaks $C_{M,j}$ for $j \in \{1, ..., n_{peaks}\}$ in $M_Q(t)$ via $k-$means clustering. Then, each robot navigates towards the nearest cluster centroid of $M_Q(t)$. Upon reaching a centroid, we update the clusters and choose a new target. Algorithm 2 summarizes this approach. Simulations presented in Section IV demonstrate this is an effective algorithm for one or more robots in the environment.

Algorithm 2 Voronoi-Based UVC Adaptive Coverage

```
Update Estimate of Dosage Required φ_D(q,t) (7)
Update Mass M_Q(t) (8)
Find Peaks in Mass, C_{M,j} via clustering
for i ∈ n robots at positions p_i do
    Update Voronoi Cell V_i
    Determine nearest C*_{M,j} = min_j ||C_{M,j} − p_i||
    if ||C*_{M,j} − p_i|| < ε then
        Update Peaks in Mass, C_{M,j}, via clustering
    if C*_{M,j} ∈ V_i then
        Move towards point ṗ_i = k (p_i − C*_{M,j})
    else
        Find nearest point in V_i to C*_{M,j} and move towards that point
    Update dosage applied D^τ(p_i, V_i, t) (2)
```

IV. Simulations

In this Section, we present our simulation results for the Adaptive Voronoi-Based Coverage approach summarized in Algorithm 2. We propose that a robot provide adaptive UVC dosage to an environment with random obstacles following a technique that decreases the total mass in the environment, where the mass is calculated from remaining dosage requirements. This approach works for one or more agents operating in a space. Figure 4 illustrates a group of $n = 4$ robots in an environment with obstacles performing Algorithm 2.

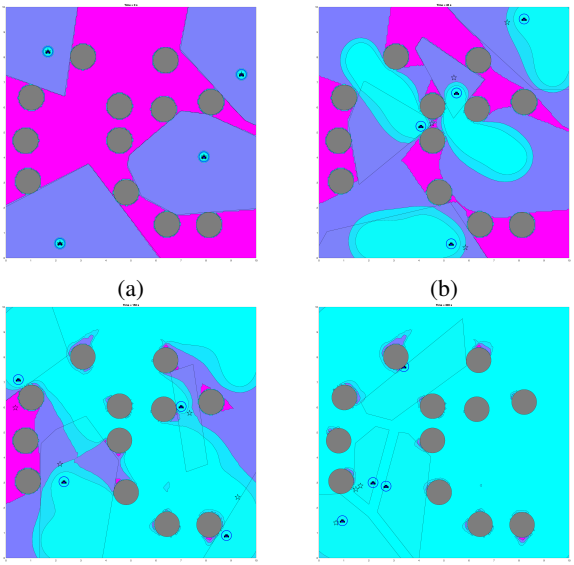

(a) (b) (c) (d)

Fig. 4: Robots performing Voronoi-based adaptive coverage can dynamically apply UVC dosage to an environment with obstacles. The remaining dosage requirement $\phi(q,t)$ is shown in the color scale, with pink and purple indicating dosage needed. At each time step, the robots calculate the remaining dosage requirements in $\phi(q,t)$ by subtracting their individual dosage applied within their Voronoi cell. Over time, our algorithm drives the robots to explore the dosage and provide all areas with a sufficient dosage (bright blue).

Here, the agents use the Obstacle-Aware Voronoi Tessellation [37], which increases the area of their individual cell to be tangential with obstacle borders. At each time step, robots estimate their UVC dosage delivery by applying (2) over their individual Voronoi cell. This is a conservative approximation to address occlusions from obstacles. In Figure 4, the contours within the environment denote the total applied dosage. Here, we specify a target dosage of 5 mJ/cm^2, shown as bright blue. Our policy drives the robots to explore and disperse through the environment, and as $\phi_D(q,t)$ evolves, it will drive agents to new areas that need UVC within the environment. By the final point in time, the robots have delivered the target dosage to all points in the environment.

We verify the performance of the robots by examining the total mass $M_Q(t)$ over time in Figure 5. Figure 5a plots $M_Q(t)$ for twenty trials with $n = 4$ UVC robots and 12 obstacles. The obstacles and the robots have randomized initial positions. We observe that the final mass in all trials goes to zero, indicating that the target dosage has been applied to all points of interest in the environment. Figure 5b compares the average time to 2% mass remaining for varying numbers of robots. Each box plot in Figure 5b represents twenty randomized trails with 12 obstacles. We notice that the average time to $0.02M_Q$ decreases with the number of robots on the team.

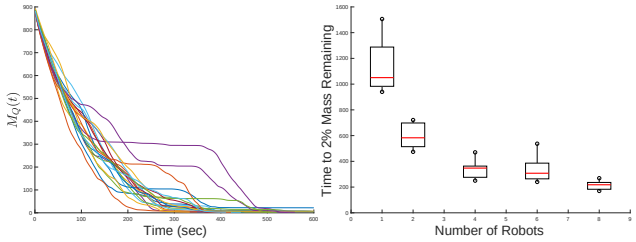

(a) (b)

Fig. 5: (a) $M_Q(t)$ over time for 20 trials of $n = 4$ robots and 12 randomized obstacles. (b) A comparison of the time to $0.02M_Q$ for varying numbers of robot teams in an environment with 12 randomized obstacles.

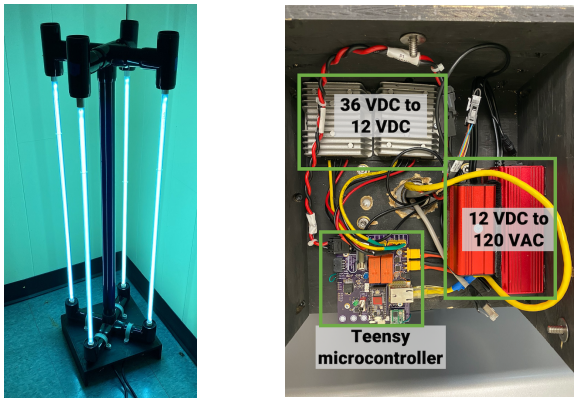

(a) UVC Lamps (b) Relay Board

Fig. 6: (a) Custom UVC Lamp assembly that mounts atop the Ava mobile base. (b) Power relay and Teensy microcontroller for controlling the lamps.

V. Platform Overview

This section details the main components of the physical system at The GBFB. The motivation for designing this robot was to create a mobile UVC disinfection robot for deployment at The GBFB during the COVID-19 pandemic. Design work began in April 2020, with delivery to The GBFB in early June 2020. These implementation decisions enabled rapid prototyping and deployment, and accounted for reduced availability of parts and a remote team integration during the pandemic. Our system contains three key components: (i) the Ava Robotics mobile base, (ii) a custom UVC lamp assembly, and (iii) an Arduino-powered relay board that controlled the UVC lamp assembly from remote and base commands. In addition, for our deployment at The Greater Boston Food Bank, we created a remote alarm integration to act as a secondary emergency shut-off.

A. AVA Robotics Mobile Base

We chose the Ava Robotics base as our mobile platform[1]. The base has a holonomic drive system with a maximum moving speed of 1 m/s and a minimum speed of 0.1 m/s. It is equipped with 2D lidars, which enable SLAM-based navigation, on-board odometry, and front-facing depth cameras

[1]http://avarobotics.com

Distance (m)	Est Intensity $\alpha = 3.0e6$ ($\mu W/cm^2$)	Avg. Intensity ($\mu W/cm^2$)	Extrapolated α (μW)
0.81	457	484	3.17e6
1.11	243	278	3.46e6
1.42	149	188	3.79e6
2.03	73	104	4.30e6
2.64	43	66	4.59e6
3.25	28	45	4.75e6

TABLE I: Measured UVC intensity values of our payload, and predicted α values.

for dynamic collision avoidance. The base provides 36VDC power to payloads, and Ethernet communication with its onboard Linux computer. Remote management, including tele-operation, is provided through Ava's web servers. The robot self-charges its batteries between patrols on its dock.

B. UVC Lamp Assembly

Our assembly comprises four UVC lamps, arranged in a radial configuration, as shown in Figure 6a. Each lamp is rated for 16W of 254nm UV output, with an intensity of 150 μW/cm^2 at a one meter distance[2]. Two 120 VAC ballasts drive the lamps. The PVC frame enabled rapid assembly and encloses all electrical wiring. For dosage calculations in path planning and reporting, we assume that the dosage provided by the entire payload is equivalent to two individual lamps for any point around the robot, with $\alpha = 3.0e6$ μW. A UVC dosimeter verified our system provided its expected UVC intensity, and that the intensity is radially symmetric around the robot. We also note that while our measured intensity values did not exactly follow an inverse-squared distance relationship described in Section II, it never over-estimates the performance. Table I summarizes our recorded average intensity values at various distances from the robot.

C. Relay Board Design

The Ava mobile base provides 36 VDC power for external payloads and Ethernet for communication. The electronic control system serves two purposes: (i) convert Ava's base power to the 120 VAC needed to drive the UVC ballasts; and (ii) actuate the UVC lamps with several layers of redundancy. A prototype system was quickly designed and fabricated, shown in Figure 6b. For communication, the system uses a Teensy 3.2 micro-controller[3] connected through SPI to a WIZ850IO SPI-based Ethernet module to communicate with the base, as well as a RFM69HCW short-range wireless radio for remote control. In order to simplify the design, the power system was split up into two parallel systems (one for each UVC ballast), which allowed for the use of lower-current rated components. The power system first steps down the 36 VDC to 12 VDC with a DC-DC Converter, enabling us to use off-the-shelf 120 VAC inverters. Then the microcontroller controls the state of the lights through two relays.

[2]Datasheet provided by American Ultraviolet, manufacturer and supplier of the UVC lamps

[3]https://store.arduino.cc/usa/teensy-3-2-usb-development-board

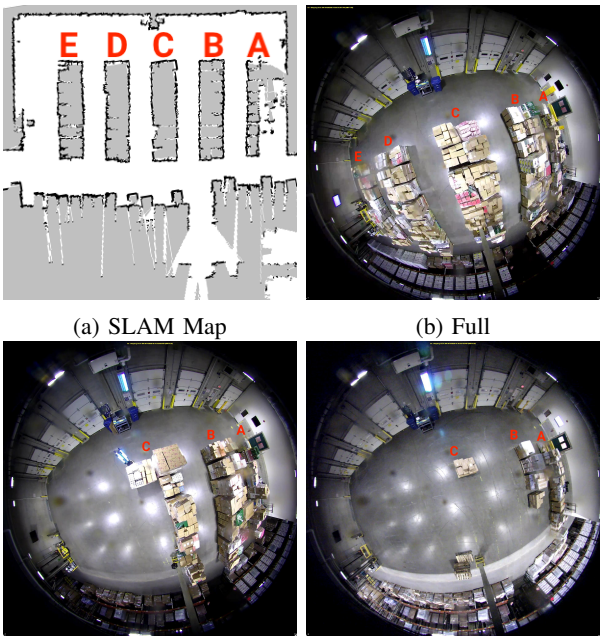

(a) SLAM Map (b) Full

(c) Half-Full (d) Almost Empty

Fig. 7: The number of aisles to disinfect at the Greater Boston Food Bank varied from run to run. The SLAM map in (a) corresponds to a "full" staging area, shown in (b), but at times the dock could be (c) half-full, or (d) almost-empty.

D. Remote Shut-Off and Alarm Integration

Because UVC light is harmful humans, we wanted to ensure that the robot would stop patrolling if an unexpected person entered the building. Using an existing door monitoring system as a trigger mechanism, we can send a high priority push notification to the robot ordering it to shut off its lights if tripped. Additionally, a wireless remote can also be used to disable the UVC lamps.

VI. Deployment and Experiments at The Greater Boston Food Bank

Our robot was first delivered to The GBFB in June 2020 with the objective to perform nightly patrols for exposed surface and aerosol disinfection. During June and July 2020, the robot performed a mix of tele-operated patrols and autonomous patrols. This allowed us to verify the UVC disinfection function of the robot and its safe navigation capabilities. The robot switched to all-autonomous patrols by August 2020. The experimental results summarize over 50 autonomous patrols conducted between August and October 2020[4]. Patrols did not run on days when nothing was staged for distribution, and for approximately three weeks in August and September due to infrastructure work at The GBFB.

A. Environment Layout

The robot was tasked to patrol the staging area of The GBFB, which is seen in Figure 1 and in the camera view in

[4]In November 2020, the robot prototype was upgraded with a newer version that contained significant design and feature changes. Experiments with this updated robot are still ongoing, and are therefore not included in this paper.

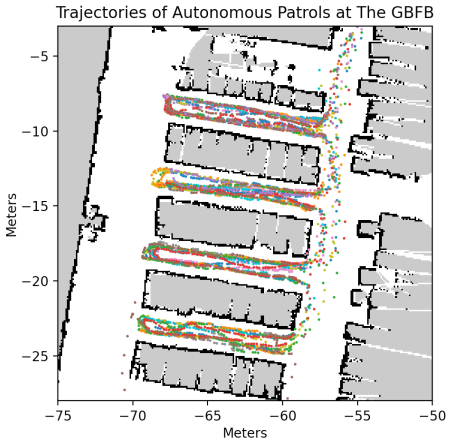

Fig. 8: For each patrol, the robot relies on its static SLAM map to navigate the aisles. We plot the trajectory data for 16 patrols performed during October 2020.

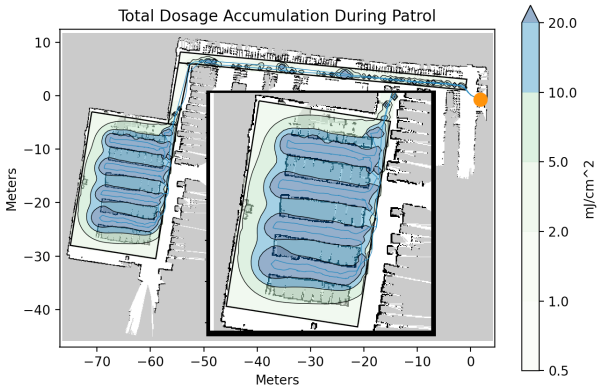

Fig. 9: Total dosage delivered by the robot during patrol. The aisles of pallets are shown as grey rectangles, and the dock is marked in orange. The robot traverses from the rear of the warehouse to the staging area and back.

Figure 7. The staging area at The Greater Boston Food Bank is about 4000 ft^2 (400 m^2) and contains up to five aisles of pallets. Although not all aisles may be occupied on any given day, we achieved reliable and repeatable performance with a static SLAM map that includes the aisles as obstacles, seen as the grey rectangles in Figure 8. The robot constructed an onboard SLAM map from its 2D lidars prior to performing its autonomous patrols. During patrols, the robot uses both its lidar as well as the depth cameras for local collision avoidance around pallets and obstacles that may shift from day to day. No external sensors or information is used for navigation or localization; the camera view in Figure 7 is a security camera that is not integrated with the robot.

B. Patrol Design

As shown in Figure 7, the staging dock contains up to five aisles of pallets staged for pickup the next day. We treat these aisles as obstacles for navigation, and designed a fixed patrol route with a fixed speed of 0.1 m/s as the robot drives in the staging area. Although the pallets are navigation obstacles, the lights on the robot are designed to be taller than the height of the aisles, and we treat the staging area as a single continuous convex region for our estimate of UVC delivery.

Our goal is to provide UVC disinfection between shifts of workers, targeting aerosol particles lingering in the air and droplets that have fallen on the floor and pallet tops. During the staging process, pre-packaged pallets are driven to the staging dock, thus our focus is not on disinfecting all sides of a pallet, nor all its contents. It is instead focusing on the droplets that fall from the air and become surface fomites on the remaining exposed surfaces. As mentioned in Section II, at the point of deployment in June 2020, we targeted a dosage of 10 mJ/cm^2. We designed a static patrol route to navigate up and down the aisles, such that in a single up-and-down pass of an aisle, the robot delivers the target dosage to the nearby volume. This patrol design was inspired by our static path plans from Section III, as well as Cellular Decomposition strategies in [14], [15].

These experiments ran nightly and launched autonomously when the building was not occupied. However, as not all aisles were occupied on any given day, a human user could specify the aisles to visit before a patrol, and the path would update accordingly. Trajectory data from 16 patrols performed during October 2020 are plotted in Figure 8.

C. Disinfection Results

As discussed in Section II, our target UVC dosage was 10 mJ/cm^2. Although the aisles appear as obstacles in the SLAM map, the UVC lamp assembly is positioned above the tops of the pallets. For the purposes of UVC dosage accumulations, we treat the staging area as a continuous convex region, as the lights of the robot are not occluded by the pallets. Figure 9 plots the contours of the dosage accumulation during a robot patrol of four aisles A-D (aisle E was not full during this patrol). The robot achieves its target dosage of 10 mJ/cm^2 across the aisles, with maximum dosage values exceeding 20 mJ/cm^2. The time to complete the patrol was 20 min, with the robot moving at a decreased speed of 0.1 m/s in the staging area. These results suggest we achieve at least D_{99} dosages to mitigate both surface fomites and airborne particles of SARS-CoV-2.

VII. Conclusions

This paper presents our algorithms, platform, and experimental results for mobile UVC disinfection robot. Our robot was deployed at The Greater Boston Food Bank (GBFB), where we performed patrols of the warehouse staging area and delivered dosages of at least 10mJ/cm^2 to the aisles of pallets in the staging area. We discuss our model of UVC disinfection for a mobile robot, and simulations illustrate how this problem can be generalized multi-robot applications and adaptive coverage. Future work will look to refine our UVC dosage model, explore other applications of Ultraviolet Germicidal Irradiation (UVGI), extending to further online, adaptive planning policies.

ACKNOWLEDGMENTS

The authors would like to thank the following: Richard Ghiz and The Greater Boston Food Bank team; Marcio Macedo, Youssef Saleh, and the team at Ava Robotics;

Saman Amarasinghe, Bryan Teague, Igor Gilitschenski, and Xiao Li. Ava Robotics also donated the mobile base for The GBFB deployment, we are grateful for their support.

REFERENCES

[1] N. G. Reed, "The history of ultraviolet germicidal irradiation for air disinfection," *Public health reports (Washington, D.C. : 1974)*, vol. 125, no. 1, pp. 15–27, 2010, 20402193[pmid]. [Online]. Available: https://pubmed.ncbi.nlm.nih.gov/20402193

[2] B. R. Yaun, S. S. Sumner, J. D. Eifert, and J. E. Marcy, "Inhibition of pathogens on fresh produce by ultraviolet energy," *International Journal of Food Microbiology*, vol. 90, no. 1, pp. 1 – 8, 2004. [Online]. Available: http://www.sciencedirect.com/science/article/pii/S0168160503001582

[3] S. Cremers-Pijpers, C. van Rossum, H. Wertheim, A. Tostmann, and J. Hopman, "Disinfecting handheld electronic devices with uv-c in a healthcare setting." *medRxiv*, 2020. [Online]. Available: https://www.medrxiv.org/content/early/2020/04/06/2020.04.01.20048496

[4] A. Guridi, E. Sevillano, I. de la Fuente, E. Mateo, E. Eraso, and G. Quindós, "Disinfectant activity of a portable ultraviolet c equipment," *International journal of environmental research and public health*, vol. 16, no. 23, p. 4747, Nov 2019, 31783593[pmid]. [Online]. Available: https://pubmed.ncbi.nlm.nih.gov/31783593

[5] G. Paslakis, G. Dimitropoulos, and D. K. Katzman, "A call to action to address COVID-19–induced global food insecurity to prevent hunger, malnutrition, and eating pathology," *Nutrition Reviews*, 07 2020, nuaa069. [Online]. Available: https://doi.org/10.1093/nutrit/nuaa069

[6] C. E. Ochoa-Velasco, R. Ávila-Sosa, P. Hernández-Carranza, H. Ruíz-Espinosa, I. I. Ruiz-López, and J. Á. Guerrero-Beltrán, "Mathematical modeling used to evaluate the effect of uv-c light treatment on microorganisms in liquid foods," *Food Engineering Reviews*, vol. 12, no. 3, pp. 290–308, Sep 2020. [Online]. Available: https://doi.org/10.1007/s12393-020-09219-y

[7] A. A. Gabriel and H. Nakano, "Inactivation of salmonella, e. coli and listeria monocytogenes in phosphate-buffered saline and apple juice by ultraviolet and heat treatments," *Food Control*, vol. 20, no. 4, pp. 443 – 446, 2009. [Online]. Available: http://www.sciencedirect.com/science/article/pii/S0956713508002193

[8] S. N. Rudnick, "Predicting the ultraviolet radiation distribution in a room with multilouvered germicidal fixtures," *AIHAJ*, vol. 62, no. 4, pp. 434–445, Aug 2001 Jul, copyright - Copyright American Industrial Hygiene Association Jul/Aug 2001. [Online]. Available: https://search.proquest.com/docview/236210626?accountid=12492

[9] W. G. Lindsley, T. L. McClelland, D. T. Neu, S. B. Martin Jr., K. R. Mead, R. E. Thewlis, and J. D. Noti, "Ambulance disinfection using ultraviolet germicidal irradiation (uvgi): Effects of fixture location and surface reflectivity," *Journal of occupational and environmental hygiene*, vol. 15, no. 1, pp. 1–12, Jan 2018, 29059039[pmid]. [Online]. Available: https://pubmed.ncbi.nlm.nih.gov/29059039

[10] A. R. Sambol and P. C. Iwen, "Biological monitoring of ultraviolet germicidal irradiation in a biosafety level 3 laboratory," *Applied Biosafety*, vol. 11, no. 2, pp. 81–87, 2006. [Online]. Available: https://doi.org/10.1177/153567600601100204

[11] J. J. McDevitt, S. N. Rudnick, and L. J. Radonovich, "Aerosol susceptibility of influenza virus to uv-c light," *Applied and environmental microbiology*, vol. 78, no. 6, pp. 1666–1669, Mar 2012, 22226954[pmid]. [Online]. Available: https://pubmed.ncbi.nlm.nih.gov/22226954

[12] M. W. First, E. A. Nardell, W. Chaisson, and R. Riley, "Guidelines for the application of upper-room ultraviolet germicidal irradiation for preventing transmission of airborne contagion – part 1: Basic principles," 7 1999.

[13] T. Leach and R. Scheir, "Ultraviolet germicidal irradiation (uvgi) in hospital hvac decreases ventilator associated pneumonia," *ASHRAE Transactions*, vol. 120, Jan 2014, 1. [Online]. Available: https://link.gale.com/apps/doc/A371282999/AONE?u=mlin_b_massblc&sid=AONE&xid=d381879a

[14] H. Choset, "Coverage of known spaces: The boustrophedon cellular decomposition," *Autonomous Robots*, vol. 9, no. 3, pp. 247–253, Dec 2000. [Online]. Available: https://doi.org/10.1023/A:1008958800904

[15] S. Brown and S. L. Waslander, "The constriction decomposition method for coverage path planning," in *2016 IEEE/RSJ International Conference on Intelligent Robots and Systems (IROS)*, 2016, pp. 3233–3238.

[16] A. Khamis, A. Hussein, and A. Elmogy, *Multi-robot Task Allocation: A Review of the State-of-the-Art*. Cham: Springer International Publishing, 2015, pp. 31–51. [Online]. Available: https://doi.org/10.1007/978-3-319-18299-5_2

[17] N. Mathew, S. L. Smith, and S. L. Waslander, "Planning paths for package delivery in heterogeneous multirobot teams," *IEEE Transactions on Automation Science and Engineering*, vol. 12, no. 4, pp. 1298–1308, 2015.

[18] T. Sakamoto, S. Bonardi, and T. Kubota, "A routing framework for heterogeneous multi-robot teams in exploration tasks," *IEEE Robotics and Automation Letters*, vol. 5, no. 4, pp. 6662–6669, 2020.

[19] S. L. Smith, M. Schwager, and D. Rus, "Persistent robotic tasks: Monitoring and sweeping in changing environments," *IEEE Transactions on Robotics*, vol. 28, no. 2, pp. 410–426, 2012.

[20] A. Ulusoy, S. L. Smith, X. C. Ding, C. Belta, and D. Rus, "Optimality and robustness in multi-robot path planning with temporal logic constraints," *The International Journal of Robotics Research*, vol. 32, no. 8, pp. 889–911, 2013.

[21] N. Mathew, S. L. Smith, and S. L. Waslander, "Multirobot rendezvous planning for recharging in persistent tasks," *IEEE Transactions on Robotics*, vol. 31, no. 1, pp. 128–142, 2015.

[22] A. Sadeghi, A. B. Asghar, and S. L. Smith, "On minimum time multi-robot planning with guarantees on the total collected reward," in *2019 International Symposium on Multi-Robot and Multi-Agent Systems (MRS)*, 2019, pp. 16–22.

[23] J. Cortes, S. Martinez, T. Karatas, and F. Bullo, "Coverage control for mobile sensing networks," *IEEE Transactions on Robotics and Automation*, vol. 20, no. 2, pp. 243–255, 2004.

[24] M. Schwager, D. Rus, and J.-J. Slotine, "Decentralized, adaptive coverage control for networked robots," *The International Journal of Robotics Research*, vol. 28, no. 3, pp. 357–375, 2009. [Online]. Available: https://doi.org/10.1177/0278364908100177

[25] J. Cortés and M. Egerstedt, "Coordinated control of multi-robot systems: A survey," *SICE Journal of Control, Measurement, and System Integration*, vol. 10, no. 6, pp. 495–503, 2017.

[26] J. Tardós, R. Aragues, C. Sagüés, and C. Rubio, "Simultaneous deployment and tracking multi-robot strategies with connectivity maintenance," *Sensors*, vol. 18, no. 3, 2018. [Online]. Available: https://www.mdpi.com/1424-8220/18/3/927

[27] Xenex. (2020) Germ-zapping robots: Uv disinfection technology for your cleaning teams. Accessed October 31,2020. [Online]. Available: https://go.xenex.com/PXUV-disinfection.html

[28] S. U. Technology. (2020) Surfacide uv-c decontamination. Accessed October 31,2020. [Online]. Available: https://www.surfacide.com/

[29] U. Robots. (2020) Uvd robots revolutionizing disinfection. Accessed October 31,2020. [Online]. Available: https://www.uvd-robots.com/

[30] SmartGuardUV. (2020) Smartguarduv automates & performs smart disinfection for your facility. Accessed October 31,2020. [Online]. Available: https://smartguarduv.com/products/

[31] H. Chick, "An investigation of the laws of disinfection," *Journal of Hygiene*, vol. 8, no. 1, p. 92–158, 1908.

[32] M. Heßling, K. Hönes, P. Vatter, and C. Lingenfelder, "Ultraviolet irradiation doses for coronavirus inactivation - review and analysis of coronavirus photoinactivation studies," *GMS hygiene and infection control*, vol. 15, pp. Doc08–Doc08, May 2020, 32547908[pmid]. [Online]. Available: https://pubmed.ncbi.nlm.nih.gov/32547908

[33] C. M. Walker and G. Ko, "Effect of ultraviolet germicidal irradiation on viral aerosols," *Environmental Science & Technology*, vol. 41, no. 15, pp. 5460–5465, Aug 2007. [Online]. Available: https://doi.org/10.1021/es070056u

[34] N. Storm, L. McKay, S. Downs, R. Johnson, D. Birru, M. de Samber, W. Willaert, G. Cennini, and A. Griffiths, "Rapid and complete inactivation of sars-cov-2 by ultraviolet-c irradiation," *Research Square*, Oct 2020. [Online]. Available: https://doi.org/10.21203/rs.3.rs-65742/v1

[35] A. Bianco, M. Biasin, G. Pareschi, A. Cavalleri, C. Cavatorta, C. Fenizia, P. Galli, L. Lessio, M. Lualdi, E. Redaelli, I. Saulle, D. Trabattoni, A. Zanutta, and M. Clerici, "Uv-c irradiation is highly effective in inactivating and inhibiting sars-cov-2 replication," *medRxiv*, 2020. [Online]. Available: https://www.medrxiv.org/content/early/2020/06/23/2020.06.05.20123463

[36] H. Inagaki, A. Saito, H. Sugiyama, T. Okabayashi, and S. Fujimoto, "Rapid inactivation of sars-cov-2 with deep-uv led irradiation," *Emerging Microbes & Infections*, vol. 9, no. 1, pp. 1744–1747, 2020, pMID: 32673522. [Online]. Available: https://doi.org/10.1080/22221751.2020.1796529

[37] A. Pierson and D. Rus, "Distributed target tracking in cluttered environments with guaranteed collision avoidance," in *2017 International Symposium on Multi-Robot and Multi-Agent Systems (MRS)*, 2017, pp. 83–89.